Continuous fluorescence microphotolysis to observe lateral diffusion in membranes. Theoretical methods and applications

Axel Brünger[a)]
Technische Universität München, Physik Department, D 8046 Garching, Federal Republic of Germany

Reiner Peters
Max-Planck Institut für Biophysik, D 6000 Frankfurt/Main 71, Federal Republic of Germany

Klaus Schulten
Technische Universität München, Physik Department, D 8046 Garching, Federal Republic of Germany

(Received 11 May 1984; accepted 3 August 1984)

On the basis of solutions to two-dimensional diffusion-reaction equations the fluorescence signal for photobleaching experiments with arbitrary time-dependent and time-independent irradiation profiles is evaluated. The solutions involve spatial discretization and spectral expansion, spatial and temporal discretization employing the Crank–Nicholson integration scheme, generalized moment expansion, and an approximation yielding an analytical expression. The algorithms developed can be installed on small computers to determine lateral diffusion coefficients from observed fluorescence signals. The theory developed is applied to photobleaching with constant irradiation profiles and the resulting diffusion coefficients, in the range 0.001 to 10.0 $\mu m^2 s^{-1}$ for the systems investigated, are compared to the results of conventional photobleaching experiments. Applications of the theory compare further the signals resulting from Gaussian and rectangular irradiation profiles, the influence of the membrane geometry, i.e., planar or spherical, on the fluorescence signal, and the effect of finite diffusion spaces.

I. INTRODUCTION

Many biochemical reactions of the living cell are controlled by the time which biomolecules, in search of their target, spend on Brownian motion. This time is determined largely by the topology of the spaces in which the Brownian motion of biomolecules is carried out. In order to increase the respective reaction rate constants diffusion controlled reaction processes are often confined to spaces of low effective dimension, e.g., to the plane of two-dimensional membranes or along one-dimensional polymers. For an understanding of this regulation of diffusion-controlled processes it is most important to measure the transport properties of biological materials, preferably in the living cell. A most important contribution to this goal has come through the development of the photobleaching method, often referred to as fluorescence microphotolysis (FM) or fluorescence recovery after photobleaching (FRAP).[1–4]

Observation of the transport properties also reveal information on the structure of the molecular environment to which biomolecules investigated are confined. In case of a membrane environment the membrane lipids form a bilayer which together with the membrane proteins have been considered a two-dimensional viscous liquid.[5] The lateral diffusion of membrane constituents is determined in part through their geometry and the viscosity of the membrane. However, connection of the membrane to the cytoplasmic structures within the cell or the formation of heterogeneous lipid areas can also contribute to the mobility in cellular membranes.[4] Examples of structure-transport relationships have been found in connection with the phase transition of DMPC vesicles (see Sec. III A), with the influence of the spectrin–actin network in the diffusion of proteins in erythrocytes,[1,4] and with the effect of membrane inhomogeneities on lipid diffusion.[6]

So far a relationship between biological function and lateral transport in membranes could be demonstrated only for a few systems. Examples for membrane processes controlled by lateral diffusion are the reactions of the electron transport systems in microsomal membranes,[7] the hormonal stimulation of adenylcyclase,[8] and hormone-induced clustering of membrane proteins.[9]

To apply the photobleaching method the biomolecules of interest, so far mainly constituents of biological membranes, are labeled by suitable fluorescent dyes. In order to investigate the diffusion of lipids one introduces lipid-like fluorophores, e.g., DiO (see Sec. III A) into the membranes. If one wishes to monitor the diffusion of membrane proteins one labels these particles either unspecifically by reaction with a fluorescent reagent like FITC (see Sec. III A) or specifically by introduction of fluorescent antibodies, toxins or hormones. The dyes employed need to have the property that radiation produces fluorescence as well as a photoreaction resulting in a nonfluorescent product. This property provides the basis of the photobleaching method.

In the conventional application of the photobleaching method (FM or FRAP) a small area of a membrane (a few μm^2) is irradiated by an intense laser pulse (1–100 mW). As a result most of the dyes in the irradiated area (IA) are photolyzed to a nonfluorescent product. Little fluorescence will be detected from the IA at this moment. In a second phase the diffusion of nonphotolyzed dyes into the IA is monitored by means of an attenuated laser beam (10–10 000 nW). The intensity of this beam just suffices to monitor by means of a single photon counting equipment the fluorescence of the fresh dyes in the IA. However, the intensity is chosen small

[a)] Current address: Max-Planck Institut für Biochemie, D 8033 Martinsried, Federal Republic of Germany.

 0021-9606/85/042147-14$02.10

enough to avoid significant photolysis. The recovery of the fluorescence signal from an initial zero value is recorded and analyzed to yield the diffusion coefficient of the fluorophores.[1,2] The intensity pattern (strong/weak) is chosen mainly because of the convenience of the mathematical analysis of the fluorescence recovery curve: The problem of diffusional reentrance into an area with either rectangular or Gaussian concentration profile yields an analytical solution.[1,2,10,11] In this paper we suggest the application of arbitrary intensity patterns which require, however, a more involved analysis of the observed fluorescence signal. In order to facilitate corresponding experiments we provide some numerical and approximate analytical solutions which can be compared with the observed signals. Actually, variants of the conventional FM and CFM photobleaching method involving different irradiation geometries have been suggested previously.[12] However, these variants are still based on consecutive strong (bleaching) and weak (fluorescence monitoring) intensity periods.

There are several reasons why more general intensity patterns are desirable for photobleaching experiments. One reason relates to the requirement of a sensitive photon detecting device and an intense (laser) light source for an FM experiment. Another reason lies in the need of sufficient fluorophore concentrations to produce enough fluorescence in the weak intensity phase. A third reason is connected with certain idealized assumptions for analysis of FM experiments, namely that fluorophore transport can be neglected during the bleaching phase; this condition may be violated for systems with high mobility.

The difficulties mentioned can be avoided if one applies, at the cost of a more difficult analysis of the fluorescent signal, a medium, but constant light intensity (about $10\,\mu$W) to the irradiated area. This variant of the photobleaching method termed "continuous fluorescence microphotolysis" (CFM) has been introduced by us recently.[13] We have demonstrated the functionality of this method, but did not describe the mathematical algorithm needed for the analysis for the fluorescence signal in detail. This information, applicable in fact to more general intensity patterns than considered in Ref. 13, will be provided in this paper.

In Secs. II A and II B, the theory of photobleaching processes is formulated in terms of diffusion-reaction equations on planar, as well as on spherical surfaces and expressions for the relevant observables are derived. In Sec. II C, a spatial discretization scheme is introduced which facilitates an evaluation of the fluorescence signal as shown in Sec. II D. In Sec. II E we introduce an alternative algorithm based on a spatial as well as temporal discretization scheme; this description covers experiments with time-dependent intensity patterns. Section II F provides an analysis of the long-time behavior of the fluorescence signal. In Sec. II G we furnish a generalized moment expansion of the fuorescence signal which provides the fastest method for an exact evaluation of the signal for comparison with the observation. Section II H introduces an approximate analytical description of the fluorescence signal which is suitable for fast, but approximate calculations.

Section III provides several applications of the CFM method. Since the potential of the CFM method has been illustrated before,[13] this section addresses mainly those aspects which are concerned with the theoretical basis of the method. However, in Sec. III A we show that diffusion coefficients ranging from 0.001 to 10.0 $\mu m^2 s^{-1}$ are determined reliably by the CFM method. In Sec. III B we compare applications with Gaussian and rectangular intensity profiles. In Sect. III C we will discuss the effect of the membrane geometry, i.e., planar or spherical, on the CFM signal. Section III D shows that the theory developed can be applied to conventional FM photobleaching. In particular, we will discuss the problem of an immobile fraction of fluorophores. Section III E addresses the convergence property of the generalized moment expansion of the fluorescence signal and Sec. III F the implementation of the suggested algorithms on lab computers.

II. METHODS

A. Concept and observable

The fluorescence signal of a CFM experiment (see, e.g., Figs. 2(b) and 2(c)] serves as a measure of the concentration of nonphotolyzed fluorophores in the IA (IA = irradiated area). The signal exhibits an initial fast decay followed by a slower decay. The fast decay reflects the photolysis of fluorophores initially located in the IA, the slow decay reflects the depletion of fluorophores from parts distant of the IA which have entered the IA by diffusion. The fit between observation and an appropriate model is the basis of the CFM method and yields the diffusion coefficient D of the fluorescent species. Efficient theoretical methods to simulate the model had to be developed and will be described in the following sections.

The experimental CFM apparatus used in this work is the same as described in Ref. 13. It consists of a fluorescence microscope, a single-photon counting system, an argon laser, a shutter, and other optical devices. In the following a short summary of the experimental procedure is given, for a more detailed description one may refer to Ref. 13. After passing some optical devices the laser beam is imaged into the microscope and then irradiates the IA on the membrane. Within certain limits the size, shape, and intensity of the IA can be selected. While suppressing the direct laser scatter beam by a dichromatic beam splitter, the time dependence of the emitted fluorescence is monitored by a photomultiplier. To obtain a measure of the number of active fluorophores in the IA, the integral number of fluorescence photons within consecutive equal-time intervals is detected and averaged over the intervals.

B. Description of the CFM model

Excitation of a fluorophore C leads either to fluorescence or less likely to irreversible photolysis of the fluorophore. The product P of this reaction is inactive, i.e., does not fluoresce anymore. We will describe this photochemical reaction as two consecutive first order processes

$$C \overset{h\nu}{\rightleftharpoons} C^* \overset{\text{photolysis}}{\longrightarrow} P.$$

In a CFM experiment the interplay between the diffusion of the unbleached chromophores C into the IA and photolysis $C \rightarrow P$ within the IA is being monitored. The time development of the concentration $P(\mathbf{r}, t)$ of nonphotolyzed fluorophores C is described then by a diffusion-reaction equation

$$\frac{\partial}{\partial t} P(\mathbf{r}, t) = l(\mathbf{r}) P(\mathbf{r}, t) - k(\mathbf{r}) P(\mathbf{r}, t), \tag{2.1}$$

where $l(\mathbf{r})$ is the (differential) diffusion operator, $k(\mathbf{r})$ the (scalar) reaction operator, and $P(\mathbf{r}, 0) = 1$ the initial distribution of the fluorophores. In Eq. (2.1), the depletion of the fluorophores by the photolysis is described by the rate constant $k(\mathbf{r})$. The spatial dependence of $k(\mathbf{r})$ is equated to the light intensity profile in the IA. As the typical irradiation in any observation amounts to about twice the characteristic diffusion time through the IA, it is sufficient to consider Eq. (2.1) only in the immediate neighborhood of the IA. Therefore, in case of a circular IA and isotropic diffusion the distribution in Eq. (2.1) is radially symmetric and the total diffusion space can be limited by a reflective boundary condition at some distance $|\mathbf{r}| = R$. This boundary condition is necessary for the numerical solution of Eq. (2.1) and, furthermore, allows to simulate the influence of a finite membrane size on the fluorescence decay curve (e.g., see Sec. III D). This is of interest as photobleaching experiments may be performed on single cells or on native membrane systems which exhibit two-dimensional compartments.[14] The influence of the three-dimensional membrane geometry on the observable will be discussed in Sec. III C (e.g., the difference of diffusion-reaction processes on flat or spherical membranes). As will be shown later the influence appears to be relatively small for CFM experiments. The radially symmetric diffusion operator and the appropriate boundary conditions for a planar geometry are

$$l(r) = D\left(\frac{\partial^2}{\partial r^2} + \frac{1}{r}\frac{\partial}{\partial r}\right) = D\,\frac{1}{r}\,\frac{\partial}{\partial r}\,r\,\frac{\partial}{\partial r},$$

$$\left.\frac{\partial}{\partial r}\right|_0 P(r, t) = \left.\frac{\partial}{\partial r}\right|_R P(r, t) = 0, \tag{2.2}$$

where D is the diffusion coefficient. For a spherical membrane geometry the center of the IA was chosen to be coincident with the lower pole of a sphere with radius S and one obtains with $r = \cos\theta$ (normalized projection onto the polar axis) instead of Eq. (2.2):

$$l(r) = \frac{D}{S^2}\,\frac{\partial}{\partial r}(1 - r^2)\frac{\partial}{\partial r},$$

$$\left.\frac{\partial}{\partial r}\right|_{-1} P(r, t) = \left.\frac{\partial}{\partial r}\right|_R P(r, t) = 0, \tag{2.3}$$

where R must be in the interval $-1 < R \leqslant 1$.

No attempt was made to incorporate the hydrodynamical interpretation of diffusion processes in membranes into our investigations. This subject and the difficulties associated with two-dimensional diffusion were discussed by Saffman and Delbrück in Ref. 15.

The intensity profile $k(r)$ is assumed to be either of rectangular or Gaussian shape corresponding to a cutoff of the central part of the laser beam or to an attenuated and focused laser beam, respectively. However, the numerical solutions described below are applicable to any profile, e.g., also to a raster intensity pattern.[12] For a rectangular profile on a flat membrane one has

$$k(r) = k_0 H(a - r), \quad 0 \leqslant r \leqslant R, \tag{2.4}$$

where k_0 is the reaction rate constant, $a < R$ is the radius of the circular IA, and $H(x)$ is the Heaviside function defined as $H(x) = 0$ for $x \leqslant 0$ and $H(x) = 1$ for $x > 0$. The Gaussian profile on a plane can be described by

$$k(r) = 2k_0 \exp(-2r^2/a^2), \quad 0 \leqslant r \leqslant R. \tag{2.5}$$

On a spherical membrane the rectangular profile is given by

$$k(r) = k_0 H(a - r), \quad -1 \leqslant r \leqslant R \leqslant 1, \tag{2.6}$$

where a is the normalized projection of the IA boundary onto the polar axis. Furthermore, the Gaussian profile on a sphere can be described by

$$k(r) = 2k_0 \exp[-2(1 + r)/(1 + a)], \quad -1 \leqslant r \leqslant R \leqslant 1, \tag{2.7}$$

which was obtained from an area conserving mapping of a Gaussian distribution onto a sphere $[r^2 \rightarrow 2S^2\pi(1 + \cos\theta_r) \approx 1 + r]$. This corresponds to a virtual deformation of an irradiated cell into a sphere. In case of equal size IA's and large R/a ratio the above profiles lead to equal total radiation doses $\int k(r)dr$.

The theoretical observable $N(t)$ in a CFM experiment is the fluorophore concentration averaged over the intensity profile in the IA:

$$N(t) = \int_{r_1}^{R} d\eta(r) P(r, t) k(r), \tag{2.8}$$

where $r_1 = 0$, $d\eta(r) = \alpha 2\pi r\,dr$ and $r_1 = -1$, $d\eta(r) = \beta 2\pi S^2 dr$ for a flat and a spherical membrane geometry, respectively. The constants α and β are chosen such that $N(0) = 1$. The actual observable N_E in the experiment is related to Eq. (2.8) by piecewise integration of $N(t)$ over some time interval τ,

$$N_E(t_i) = (1/\tau)\int_{t_i}^{t_{i+1}} dt N(t), \tag{2.9}$$

where $t_i = (i - 1)\tau$, $i = 1, 2, \ldots$.

An analytical solution of Eq. (2.1) which provides the accuracy necessary for a quantitative analysis of observation was not found in any case. In case of a planar system with rectangular intensity profile the function $k(r)$ is piecewise constant and the solution of Eq. (2.1) can be expanded into a series of zero-order Bessel functions. However, this expansion does not seem to be more efficient than the general numerical solutions described below. The discretization of the diffusion-reaction system is defined in the next section, the formal solution of the ensuing equations is given in Sec. II D. In Sec. II H will be described an analytical approximation for $N(t)$ which sufficies for an estimate of the diffusion coefficient in a CFM experiment.

C. Discretization

A finite difference approximation applied to the diffusion-reaction system (2.1) yields a master equation in a dis-

crete space ($r_1, r_2, \ldots, r_n = R$). In this approximation the Brownian motion of the fluorophores is represented by jumps between neighboring lattice points r_{i-1}, r_i, r_{i+1}. The continuous diffusion-reaction operator $l(r) - k(r)$ is replaced by a transition matrix $\mathbf{L} - \mathbf{K}$ and Eq. (2.1) is replaced by

$$\frac{\partial}{\partial t}\mathbf{P}(t) = (\mathsf{L} - \mathsf{K})\mathbf{P}. \tag{3.1a}$$

The vector $\mathbf{P}(t) = [P(r_1, t), \ldots, P(r_n, t)]$ describes the fluorophore concentration at the lattice points and obeys the obvious initial condition $\mathbf{P}(0) = (1, 1, \ldots, 1)$. The observable $N(t)$ from Eq. (2.8) is approximated by a weighted sum over the components of $\mathbf{P}(t)$:

$$N(t) = \sum_{j=1}^{n} \eta_j K_{jj} P_j(t), \tag{3.1b}$$

where the η_j correspond to the continuous measure $d\eta(r)$ in Eq. (2.8) and K_{jj} are the diagonal elements of the reaction matrix K. Suitable discretization schemes which were constructed following Refs. 16, 17, and 18 are provided for the planar as well as the spherical case in the Appendix.

D. Complete solution

The diffusion-reaction operator in Eq. (2.1) can be assumed to be time independent for CFM experiments. Therefore, the formal solution of Eq. (3.1a) can be written as

$$\mathbf{P}(t) = \exp(\mathsf{D}t)\mathbf{P}(0), \tag{4.1}$$

where $\mathsf{D} = \mathsf{L} - \mathsf{K}$. The observable $N(t)$ given in Eq. (3.1b) can also be written as

$$N(t) = \mathbf{K}^{+}\boldsymbol{\eta}\mathbf{P}(t), \tag{4.2}$$

where $\mathbf{K}$ is the diagonal of the reaction matrix K and $\boldsymbol{\eta}$ is a diagonal matrix with the elements $\eta_1, \ldots, \eta_n$. The diffusion-reaction matrix D is a nonsymmetric tridiagonal matrix which may be symmetrized by the similarity transformation S defined as a diagonal matrix with elements

$$S_{11} = 1, \quad S_{ii} = S_{i-1\,i-1}\sqrt{D_{ii-1}/D_{i-1\,i}} \tag{4.3}$$

for $n \geqslant i \geqslant 2$. Using the detailed balance condition (A5) it follows that:

$$\mathsf{S}\boldsymbol{\eta} = \eta_1 \mathsf{S}^{-1}. \tag{4.4}$$

The matrix $\tilde{\mathsf{D}} = \mathsf{S}^{-1}\mathsf{D}\mathsf{S}$ is a symmetric tridiagonal matrix with the elements

$$\tilde{D}_{ii} = D_{ii},$$
$$\tilde{D}_{ii+1} = \tilde{D}_{i+1\,i} = \sqrt{D_{ii+1}D_{i+1\,i}}\,. \tag{4.5}$$

The spectral expansion of $\tilde{\mathsf{D}}$ yields real eigenvalues λ_i and a complete system of orthonormal eigenvectors. Let $\mathsf{U} = (\mathsf{U}^{+})^{-1}$ be the orthogonal matrix containing all eigenvectors as columns. One can then represent $\tilde{\mathsf{D}}$ by

$$\tilde{\mathsf{D}} = \mathsf{U}\boldsymbol{\lambda}\mathsf{U}^{+}, \tag{4.6}$$

where $\boldsymbol{\lambda}$ is a diagonal matrix with the elements $\lambda_1, \ldots, \lambda_n$. Using $\mathsf{D} = \mathsf{S}\mathsf{U}\boldsymbol{\lambda}\mathsf{U}^{+}\mathsf{S}^{-1}$ one may write Eq. (4.1) as a sum over exponentials

$$\mathbf{P}(t) = \mathsf{S}\mathsf{U}\exp(\boldsymbol{\lambda}t)\mathsf{U}^{+}\mathsf{S}^{-1}\mathbf{P}(0)$$
$$= \sum_i \tilde{\mathbf{P}}_i \exp(\lambda_i t). \tag{4.7}$$

Similarly, one obtains for the observable $N(t)$ in Eq. (4.2),

$$N(t) = \mathbf{K}^{+}\boldsymbol{\eta}\mathsf{S}\mathsf{U}\exp(\boldsymbol{\lambda}t)\mathsf{U}^{+}\mathsf{S}^{-1}\mathbf{P}(0)$$
$$= \sum_{i=1}^{n} \exp(\lambda_i t)(\mathsf{U}^{+}\mathsf{S}\boldsymbol{\eta}\mathbf{K})_i [\mathsf{U}^{+}\mathsf{S}^{-1}\mathbf{P}(0)]_i.$$

This expression can be simplified. From Eq. (4.4) one obtains

$$\mathsf{U}^{+}\mathsf{S}\boldsymbol{\eta}\mathbf{K} = \eta_1 \mathsf{U}^{+}\mathsf{S}^{-1}\mathbf{K}$$

and since

$$\mathsf{U}^{+}\mathsf{S}^{-1}\mathbf{P}(0) = \boldsymbol{\lambda}^{-1}\mathsf{U}^{+}\mathsf{S}^{-1}(\mathsf{L} - \mathsf{K})\mathbf{P}(0)$$

and together with Eq. (A4) and $\mathsf{K}\mathbf{P}(0) = \mathbf{K}$, one gets

$$\mathsf{U}^{+}\mathsf{S}^{-1}\mathbf{P}(0) = -\boldsymbol{\lambda}^{-1}\mathsf{U}^{+}\mathsf{S}^{-1}\mathbf{K}.$$

Finally, one obtains for the observable $N(t)$,

$$N(t) = \sum_{i=1}^{n} \exp(\lambda_i t)\alpha_i,$$

where

$$\alpha_i = -(\eta_1/\lambda_i)(\mathsf{U}^{+}\mathsf{S}^{-1}\mathbf{K})_i^2$$
$$= -(\eta_1/\lambda_i)\left(\sum_{j=1}^{n} U_{ji} S_{jj}^{-1} K_{jj}\right)^2. \tag{4.8}$$

The operator L is negative definite for $\mathbf{K} \neq 0$ (see Sec. II C). This and Eq. (4.8) yields the conclusion

$$\alpha_i > 0. \tag{4.9}$$

The relations (4.8) and (4.9) can also be shown to be true for a diffusion-reaction system in an external field, where $l(\mathbf{r})$ in Eq. (2.1) is given by a Smoluchowski equation. It appears that the positivity of α_i is caused essentially by the fact that the observable $N(t)$ is determined by the reaction (intensity) profile $k(r)$. This property will be important in applying the generalized moment expansion developed in Sec. II G.

As an eigenvalue determines exactly one normalized eigenvector in a tridiagonal matrix, the eigenvalue problem for the matrix (4.6) is nondegenerate. The numerical solution was performed with an implicit QL method.[20] Equation (4.8) allows then to evaluate $N(t)$ for arbitrary times. Obviously, this method has the disadvantage to be CPU time and memory intensive ($n \approx 100$). The generalized moment expansion in Sec. II G will provide a much more efficient method for the approximate evaluation of Eq. (4.8).

E. Crank–Nicholson scheme

In addition to the spatial discretization in Sec. II C a time discretization may be introduced and the time integration be performed numerically. With the equidistant discretization of the time t,

$$t_j = (j-1)\tau, \quad j = 1, 2, \ldots$$

the Crank–Nicholson scheme[16] for the time integration can be applied,

$$\mathbf{P}(t_{i+1}) = \mathbf{P}(t_i) + 0.5(t_{i+1} - t_i)$$
$$\times(\mathsf{L} - \mathsf{K})[\mathbf{P}(t_{i+1}) + \mathbf{P}(t_i)]. \tag{5.1}$$

This implicit and recursive equation can be obtained from Eq. (3.1a) by averaging the forward and backward difference approximation of the time differential. In this way, the scheme yields a convergence in τ^2. At each time step a linear

equation has to be solved. As the diffusion operator corresponds to a tridiagonal matrix, this equation can be solved recursively. The explicit algorithm is given by the following scheme:

Initialization: (5.2a)

$$D_{nn+1} = 1.0,$$

$$c_1 = \frac{D_{12}}{-D_{11} + 2/\tau},$$

$$c_{i+1} = \frac{D_{i+1i+2}}{-c_i D_{i+1i} - D_{i+1i+1} + 2/\tau}, \quad i = 1, \ldots, n-1,$$

$$a_i = \frac{D_{ii} + 2/\tau}{D_{ii+1}}, \quad i = 1, \ldots, n,$$

$$b_{i+1} = \frac{D_{i+1i}}{D_{i+1i+2}}, \quad i = 1, \ldots, n-1,$$

$$P_1(t_0) = P_2(t_0) = \ldots = P_n(t_0) = 1, \quad P_{n+1}(t_0) = 0. \tag{5.2b}$$

Iteration:

$$d_1 = c_1[P_1(t_k)a_1 + P_2(t_k)],$$

$$d_{i+1} = c_{i+1}\{P_{i+1}(t_k)a_{i+1} + [P_i(t_k) + d_i]b_{i+1} + P_{i+2}(t_k)\}, \quad i = 1, \ldots, n-1,$$

$$P_{n+1}(t_{k+1}) = 0,$$

$$P_n(t_{k+1}) = d_n,$$

$$P_i(t_{k+1}) = d_i + c_i P_{i+1}(t_{k+1}), \quad i = n-1, \ldots, 1.$$

The algorithm allows a time dependence of the diffusion-reaction matrix D (e.g., see Sec. III D). However, in this case the coefficients a_i, b_i, c_i have to be redefined at each step. The observable can be obtained from Eq. (3.1b) at the time steps t_i. The corrected observable N_E in Eq. (2.9) can then be approximated by

$$N_E(t_i) = 0.5[N(t_i) + N(t_{i+1})].$$

The large number of time steps required for long simulation periods is a disadvantage of the Crank–Nicholson scheme. On the other hand, the algorithm allows the treatment of time-dependent diffusion-reaction systems (cf. Sec. III D) and with a small modification nonlinear reaction systems, e.g., a second order reaction term could be incorporated into Eq. (5.1) by addition of a term like

$$\mathbf{P}(t_i)\mathrm{K}^{(2)}\,\mathbf{P}(t_{i+1}).$$

F. First passage time approximation

The diffusion-reaction operator in Eq. (2.1) together with a reflective boundary condition at finite $r = R$ has a discrete, negative spectrum yielding the expansions for $P(r,t)$ and $N(t)$,

$$P(r,t) = \Sigma c_i P_i \exp(\lambda_i t),$$

$$N(t) = \Sigma A_i \exp(\lambda_i t), \tag{6.1}$$

where $A_i = c_i \int d\eta(r) P_i(r) k(r)$ and $\lambda_{i+1} < \lambda_i < \ldots < \lambda_0 < 0$. As our experience with the numerical expansion in Sec. II D has shown, the largest eigenvlaue λ_0 has always a great separation from all other eigenvalues. For a finite and not too large diffusion space this will also be true in Eq. (6.1) and at long times the λ_0 term will dominate. Hence, $P(r,t)$ and $N(t)$ show the asymptotic behavior

$$P(r,t) \approx c_0 P_0(r) \exp(\lambda_0 t),$$

$$N(t) \approx A_0 \exp(\lambda_0 t). \tag{6.2}$$

An approximate but, nevertheless, analytical expression for this eigenvalue λ_0 and the corresponding quasistationary distribution $P_0(r)$ will be derived now for the planar case (2.2) with a rectangular profile (2.4).

As $P_0(r,t) = P_0(r)\exp(\lambda_0 t)$ is a solution of the diffusion-reaction systems (2.1) and (2.4), one has

$$\left[r^2 \frac{\partial^2}{\partial r^2} + r\frac{\partial}{\partial r} - r^2(k_0 + \lambda_0)/D\right] P_0(r) = 0 \tag{6.3}$$

for $0 \leqslant r \leqslant a$, i.e., r inside the IA. As the decay of the quasistationary state $P_0(r,t)$ is diminished by diffusion from the surroundings, the absolute value of λ_0 is smaller than k_0, i.e., $1/|\lambda_0| > 1/k_0$ or $k_0 - |\lambda_0| > 0$. Since there is a reflective boundary condition at the origin, only the modified Bessel function I_0 can be a solution of Eq. (6.3),

$$P_0(r) = I_0\left(r\sqrt{\frac{k_0 + \lambda_0}{D}}\right), \tag{6.4}$$

for $0 \leqslant r \leqslant R$. Outside the IA P_0 is governed by a free diffusion problem:

$$\frac{\partial}{\partial r} P_0(r,t) = l(r) P_0(r,t), \tag{6.5}$$

where $a \leqslant r \leqslant R$. The boundary condition representing the continuity of the logarithmic derivative at the IA boundary is

$$\left.\frac{\partial}{\partial r}\right|_a P_0(r,t) = P_0(a,t)\beta\frac{I_1(\beta a)}{I_0(\beta a)},$$

where $\beta = \sqrt{(k_0 + \lambda_0)/D}$. The reflective boundary condition at large R is similar to Eq. (2.2). Using the initial condition $P_0(r,0) = P_0(r)$ one can derive a relation for λ according to the following arguments. Defining $\tilde{P}_0(r,t) = P_0(r,t)[\int_a^R d\eta(r) P_0(r)]^{-1}$ one obtains

$$\int_0^\infty dt \int_a^R d\eta(r)\tilde{P}_0(r,t) = -1/\lambda_0.$$

The left-hand side of this equation is just the first passage time τ_{fpt} for the (normalized) problem (6.5). Assuming $\tilde{P}_0(r) \approx$ const and $|\lambda_0| \ll k_0$ it follows from the theory of first passage times[21]:

$$\lambda_0 \approx \lambda_0^{\mathrm{approx}} = \left[\frac{x^2 - 3}{8} - \frac{\ln x}{2(1 - x^2)} + (1 - x^2)\sqrt{\frac{D}{k_0}}\frac{a}{2} I_0\left(a\sqrt{\frac{k_0}{D}}\right) \Big/ I_1\left(a\sqrt{\frac{k_0}{D}}\right)\right]^{-1} \tag{6.6}$$

where $x = a/R$. $\tilde{P}_0(r)$ represents the quasistationary concentration profile in the IA which the dyes assume at times longer than a^2/D and k_0^{-1}. The approximation $\tilde{P}_0(r) \approx$ const holds in case of small k_0, i.e., low measuring light intensities, a condition which should apply in situations where the long time CFM signal is not small. In Table I the accuracy of the approximation (6.6) for different ratios R/a is shown. $\lambda_0^{\mathrm{approx}}$ has been compared with the largest eigenvalue λ_0 of a complete eigenvalue evaluation (Sec. II D) of the diffusion-reac-

TABLE I. Comparison of λ_0^{approx} and the largest eigenvalue λ_0 of the diffusion-reaction operator.[a]

	$R/\mu m$			
	10.0	5.0	2.5	1.25
$k_0/(s^{-1})$				
	0.010 21	0.061 25	0.454 4	7.598
10.0	0.009 97	0.059 09	0.449 1	5.08
	0.005 269	0.025 91	0.141 4	1.531
1.0	0.005 225	0.025 36	0.130 5	0.626
	0.000 9249	0.003 926	0.018 4	0.175
0.1	0.000 9176	0.003 787	0.015 96	0.063 9
	0.000 1001	0.000 4141	0.001 898	0.017 75
0.01	0.000 0992	0.000 3977	0.001 63	0.006 39

[a] The upper values correspond to Eq. (6.6), the lower values correspond to the numerical solution (Sec. II D) of the eigenvalue problem for $j_a = 10$, $D = 1\,\mu m^2\,s^{-1}$ and $a = 1\,\mu m$ (rectangular profile).

tion operator. Good agreement is reached for a ratio $R/a \approx 10$ which is typical for CFM experiments. The inaccuracy for a smaller R/a ratio can be related to a breakdown of $|\lambda_0| \ll k_0$. The appearance of a quasistationary distribution $P_0(r)$ with time-independent shape opens the possibility of a time-integrated measurement of the two-dimensional fluorescence profile at long times. Such measurement was performed by us. A comparison of the grey level of the observed profile with $P_0(r)$ establishes a test of the theoretical description. Furthermore, one may wish to detect possible anisotropies of the fluorescence profile indicating anisotropic lateral transport in the membrane.

G. Generalized moment expansion

Interpolating the low and high frequency expansions of the CFM observable $N(t)$, a method will be developed which allows to approximate the theoretical fluorescence curve. The method is based on the Mori–Zwanzig formalism[22,23] and projects $N(t)$ onto the subspace of selected low and high frequency modes. The consideration of low frequency modes obviates the inclusion of a memory term.

1. Determination of low and high frequency modes

The evaluation will be performed for the discretized diffusion–reaction system, i.e., for the master equation (3.1a). After Laplace transformation of the expression (4.2) one obtains for the observable in frequency space

$$\hat{N}(\omega) = \int_0^\infty dt\, \exp(-\omega t) N(t) = \mathbf{K}^+ \boldsymbol{\eta} [\omega \mathbf{1} - \mathsf{D}]^{-1} \mathbf{P}(0), \tag{7.1}$$

where $\mathbf{1}$ is the unit matrix. The short time behavior (high frequency modes) of $N(t)$ is determined by the time derivatives at time $t = 0$,

$$(-1)^\nu \mu_\nu = \left.\frac{\partial^\nu}{\partial t^\nu}\right|_0 N(t) = \frac{1}{(\nu+1)!} \left.\frac{\partial^{\nu+1}}{\partial \sigma^{\nu+1}}\right|_0 \hat{N}(\omega) = \mathbf{K}^+ \boldsymbol{\eta} \mathsf{D}^\nu \mathbf{P}(0), \tag{7.2}$$

where $\sigma = 1/\omega$ and $\nu \geqslant 0$. The μ_ν will be referred to as short time moments. The long time behavior (low frequency modes) can be described by the quantities

$$\nu! \mu_{-\nu-1} = \int_0^\infty dt\, t^\nu N(t) = (-1)^\nu \left.\frac{\partial^\nu}{\partial \omega^\nu}\right|_0 \hat{N}(\omega) = (-1)^{\nu+1} \nu! \mathbf{K}^+ \boldsymbol{\eta} \mathsf{D}^{-\nu-1} \mathbf{P}(0) \tag{7.3}$$

for $\nu < 0$ and will be referred to as long time moments. Combining Eqs. (7.2) and (7.3) the moments can be expressed as matrix elements of some powers of the operator D,

$$\mu_i = (-1)^i \mathbf{K}^+ \boldsymbol{\eta} \mathsf{D}^i \mathbf{P}(0), \tag{7.4}$$

where i may be positive or negative. The moments μ_i represent the contributions of the modes $\mathsf{D}^i \mathbf{P}(0)$ to the observable. Usually, only the high frequency modes are included in the expansion. But in our case the low frequency modes actually represent the more important contributions to the observable. This will be demonstrated in Sec. III E.

For the numerical evaluation of Eq. (7.4) the vectors $\mathbf{P}_\nu$, $\mathbf{Q}_\nu$,

$$\mathbf{P}_\nu = \mathsf{D}^\nu \mathbf{P}_i^{(0)} \mathbf{Q}_\nu = \mathsf{D}^{-\nu} \mathbf{P}(0)$$

are determined in a recursive way by $\mathbf{P}_{\nu+1} = \mathsf{D}\mathbf{P}_\nu$, $\mathsf{D}\mathbf{Q}_{\nu+1} = \mathbf{Q}_\nu$, and $\mathbf{Q}_0 = \mathbf{P}_0 = \mathbf{P}(0)$. As D is a tridiagonal matrix the solution of these equations can be obtained easily. The moments μ_i may then be evaluated by use of Eq. (7.4). The cost for evaluating a single moment corresponds approximately to the evaluation of a single time step in the Crank–Nicholson scheme described in Sec. II E. The efficiency of this calculation with regard to the low frequency modes is determined by the structure of the matrix D. As a diffusive process only allows transitions between two neighboring lattice points the inversion is trivial, but in the general case the inversion may be the limiting factor for a generalized moment expansion.

2. Construction of a Padé approximant

The purpose of this section is to find a sum of exponential functions $n(t)$ with a minimum set of parameters a_i, λ_i,

$$n(t) = \sum_{i=1}^{k+m} a_i \exp(\lambda_i t), \tag{7.5}$$

whose $(2m + 2k)$ moments agree with those of the observable $N(t)$, i.e.,

$$\int_0^\infty dt\, t^\nu [N(t) - n(t)] = 0, \quad \nu = 0, 1, \ldots, 2m-1,$$
$$\left.\frac{\partial^\nu}{\partial t^\nu}\right|_0 [N(t) - n(t)] = 0, \quad \nu = 0, 1, \ldots, 2k-1. \tag{7.6}$$

Transforming Eqs. (7.5) and (7.6) into Laplace space one obtains

$$\left.\frac{\partial^\nu}{\partial \omega^\nu}\right|_0 [\hat{N}(\omega) - \hat{n}(\omega)] = 0, \quad \nu = 0, 1, \ldots, 2m-1,$$
$$\left.\frac{\partial^\nu}{\partial \sigma^\nu}\right|_0 [\hat{N}(\omega) - \hat{n}(\omega)] = 0, \quad \nu = 1, 2, \ldots, 2k, \tag{7.7}$$

where $\sigma = 1/\omega$ and $\hat{n}(\omega)$ is a rational fraction. It will be shown that $\hat{n}(\omega)$ may be represented as a $[k+m, k+m-1]$ Padé approximant in the form[22]

$$\hat{n}(\omega) = \mathbf{a}^+[\omega \mathsf{A}_1 + \mathsf{A}_2]^{-1}\mathbf{a}$$
$$= \mathbf{a}^+[\omega \mathbf{1} + \mathsf{A}_1^{-1}\mathsf{A}_2]^{-1}\mathsf{A}_1^{-1}\mathbf{a}, \tag{7.8}$$

where $\mathbf{1}$ is the unit matrix and the vector $\mathbf{a}$ and matrices A_1, A_2 are defined as

$$\mathbf{a} = \mu_{-m+i},$$
$$(\mathsf{A}_1)_{i,j} = \mu_{-2m+i+j},$$
$$(\mathsf{A}_2)_{i,j} = \mu_{-2m+i+j+1}, \tag{7.9}$$

where $i,j = 0, \ldots, k+m-1$. As is shown below the inverse in Eq. (7.8) is well defined for $m+k<n$. Furthermore, the matrix $\mathsf{A}_1^{-1}\mathsf{A}_2$ has a Frobenius normal form

$$\mathsf{A}_1^{-1}\mathsf{A}_2 = \begin{pmatrix} 0 & 0 & \ldots & 0 & \gamma_0 \\ 1 & 0 & . & & . \\ 0 & 1 & . & & . \\ . & . & & & . \\ 0 & 0 & & 1 & \gamma_{k+m-1} \end{pmatrix}, \tag{7.10}$$

where the γ_i are defined by $(\mathsf{A}_1\gamma)_i = \mu_{-m+i+k}$. Using the right-hand side of Eq. (7.8) together with Eq. (7.10) one can show that Eq. (7.7) indeed is satisfied. For the long-time moments

$$\left.\frac{\partial^\nu}{\partial \omega^\nu}\right|_0 \hat{n}(\omega) = (-1)^\nu \nu! \mathbf{a}^+(\mathsf{A}_1^{-1}\mathsf{A}_2)^{-(\nu+1)}\mathsf{A}_1^{-1}\mathbf{a},$$

one has

$$\mathsf{A}_1^{-1}\mathbf{a} = \mathbf{e}^{m+1},$$
$$(\mathsf{A}_1^{-1}\mathsf{A}_2)\mathbf{e}^{m+1} = \mathbf{e}^{m+2},$$
$$(\mathsf{A}_1^{-1}\mathsf{A}_2)^{-\nu-1}\mathbf{e}^{m+1} = \mathbf{e}^{m-\nu},$$
$$\mathbf{a}^+\mathbf{e}^{m-\nu} = \mu_{-\nu-1},$$

where $\mathbf{e}^i$ is the ith unit vector and, therefore,

$$\left.\frac{\partial^\nu}{\partial \omega^\nu}\right|_0 \hat{n}(\omega) = (-1)^\nu \nu! \mu_{-\nu-1},$$
$$\nu = 0, 1, \ldots, 2m-1.$$

Similarly, for the short-time moments holds ($\delta = 1/\omega$)

$$\left.\frac{\partial^\nu}{\partial \sigma^\nu}\right|_0 \hat{n}(\omega) = -(-1)^\nu \nu! \mathbf{a}^+(\mathsf{A}_1^{-1}\mathsf{A}_2)^{\nu-1}\mathsf{A}_1^{-1}\mathbf{a}.$$

Using $(\mathsf{A}_1^{-1}\mathsf{A}_2)^{\nu-1}\mathbf{e}^{m+1} = \mathbf{e}^{m+\nu}$ and $\mathbf{a}^+\mathbf{e}^{m+\nu} = \mu_{\nu-1}$ follows

$$\left.\frac{\partial^\nu}{\partial \sigma^\nu}\right|_0 \hat{n}(\omega) = (-1)^{\nu+1}\nu!\mu_{\nu-1}, \quad \nu = 1, \ldots, 2k.$$

3. Evaluation of the Padé approximant

The expression (7.8) is not yet suitable for practical purposes. In this section the inverse operator in Eq. (7.8) will be expanded in an orthonormal basis defined by the eigenvalue problem

$$(\lambda_\mu \mathsf{A}_1 + \mathsf{A}_2)\mathbf{b}_\mu = 0 \tag{7.11a}$$

or, equivalently,

$$(\lambda_\mu \mathbf{1} + \mathsf{A}_1^{-1}\mathsf{A}_2)\mathbf{b}_\mu = 0. \tag{7.11b}$$

For the diffusion-reaction system (3.1a), this eigenvalue problem has the following properties: (1) A_1 is positive definite; (2) the eigenvalues λ_μ are real and positive; (3) there is no degeneracy of the λ_μ; (4) the space spanned by the eigenvectors b_μ is complete; (5) Eq. (7.8) may be expanded in this space and one obtains

$$n(t) = \sum_{\mu=1}^{k+m} \exp(-\lambda_\mu t)(\mathbf{b}_\mu^+ \mathbf{a})^2/(\mathbf{b}_\mu^+ \mathsf{A}_1 \mathbf{b}_\mu). \tag{7.12}$$

In general the eigenvalue problem (7.11) may include complex eigenvalues, e.g., in systems with a threshold behavior,[24] and an expansion like Eq. (7.12) may include polynomials in the time variable t.

To prove property (1) we note that the spectral expansion (4.8) yields expressions for the moments μ_i by means of

$$\left.\frac{\partial^\nu}{\partial t^\nu}\right|_0 N(t) = \sum_{i=1}^{n} \alpha_i \lambda_i^\nu = (-1)^\nu \mu_\nu$$

for $\nu = 0, 1, \ldots, 2k-1$ and

$$\int_0^\infty dt\, t^\nu N(t) = (-1)^{\nu+1}\nu! \sum_{i=1}^{n} \alpha_i \lambda_i^{-(\nu+1)}$$
$$= \nu! \mu_{-(\nu+1)}$$

for $\nu = 0, 1, \ldots, 2m-1$. The moments can, therefore, be expressed as follows:

$$\mu_\nu = \sum_{i=1}^{n} \alpha_i (-\lambda_i)^\nu$$

for $\nu = -2m, \ldots, -1, 0, 1, \ldots, 2k-1$. Now, the positivity of the matrix A_1 can be shown:

$$\mathbf{x}^+\mathsf{A}_1\mathbf{x} = \sum_{i,j=0}^{k+m-1} x_i \mu_{-2m+i+j} x_j$$
$$= \sum_{i,j=0}^{k+m-1} \sum_{l=1}^{n} x_i x_j \alpha_l (-\lambda_l)^{-2m+i+j}$$
$$= \sum_{i,j=0}^{k+m-1} \sum_{l=1}^{n} (-\lambda_l)^{-2m} \alpha_l x_i x_j (-\lambda_l)^{i+j}$$
$$= \sum_{l=1}^{n} \alpha_l (-\lambda_l)^{-2m} \left\{ \sum_{i=0}^{k+m-1} x_i (\lambda_l)^i \right\}^2 > 0. \tag{7.13}$$

The last expression is never zero since with $\alpha_i > 0$, $\lambda_i < 0$, and $\lambda_i \neq \lambda_j$ for $i \neq j$ [see remark after Eq. (4.8)] the polynomial $p(y) = x_0 + x_1 y + x_2 y^2 + \cdots + x_{k+m-1} y^{k+m-1}$ must not have more than $(k+m-1)$ zeros. The positivity of A_2 can be shown in a similar way.

To prove property (2) we note that the positive definiteness of A_1 and A_2 implies the existence of positive, symmetric matrices F, G such that $\mathsf{A}_1 = \mathsf{F}^2$, $\mathsf{A}_2 = \mathsf{G}^2$. The eigenvalue problem (7.11) may then be written as

$$(\lambda_\mu \mathbf{1} - \mathsf{F}^{-1}\mathsf{A}_2\mathsf{F}^{-1})\mathsf{F}\mathbf{b}_\mu = 0, \tag{7.14}$$

where

$$\mathsf{F}^{-1}\mathsf{A}_2\mathsf{F}^{-1} = \mathsf{F}^{-1}\mathsf{G}\mathsf{G}\mathsf{F}^{-1} = (\mathsf{F}^{-1}\mathsf{G})(\mathsf{F}^{-1}\mathsf{G})^+.$$

It follows that the eigenvalues λ_μ are real and positive and the space spanned by the corresponding eigenvectors is complete [property (4)].

In order to show property (3) we consider the eigenvalue problem (7.11) including the Frobenius matrix $\mathsf{A}_1^{-1}\mathsf{A}_2$. The special structure of the Frobenius matrix determines exactly

one eigenvector to each eigenvalue.[19] As was already shown the eigenvectors span a complete space and, therefore, no degeneracy may occur.

Finally, property (5) will be shown. From the nondegeneracy property and by taking the difference between the equations

$$\mathbf{b}_\nu^+(\mathsf{A}_2 - \mathsf{A}_1\lambda_\mu)\mathbf{b}_\mu = 0,$$

$$\mathbf{b}_\mu^+(\mathsf{A}_2 - \mathsf{A}_1\lambda_\nu)\mathbf{b}_\nu = 0,$$

i.e.,

$$(\lambda_\nu - \lambda_\mu)\mathbf{b}_\nu^+\mathsf{A}_1\mathbf{b}_\mu = 0,$$

one obtains the relation

$$\mathbf{b}_\nu^+\mathsf{A}_1\mathbf{b}_\mu = \delta_{\nu\mu}\mathbf{b}_\nu^+\mathsf{A}_1\mathbf{b}_\nu,$$

where $\delta_{\nu\mu}$ is the Kronecker delta. Expanding $\mathsf{A}_1^{-1}\mathbf{a}$ into the complete basis set b_μ one obtains

$$\mathsf{A}_1^{-1}\mathbf{a} = \sum_\mu \beta_\mu \mathbf{b}_\mu,$$

where $\beta_\mu = (\mathbf{b}_\nu^+\mathbf{a})/((\mathbf{b}_\nu^+\ \mathsf{A}_1\mathbf{b}_\nu)$. Using

$$(\omega\mathbf{1} + \mathsf{A}_1^{-1}\mathsf{A}_2)^{-1}b_\mu = (\omega + \lambda_\mu)^{-1}\mathbf{b}_\mu$$

it follows

$$\mathbf{a}^+(\omega\mathbf{1} + \mathsf{A}_1^{-1}\mathsf{A}_2)^{-1}\mathsf{A}_1^{-1}\mathbf{a} = \sum_{\mu=1}^{n}(\omega + \lambda_\mu)^{-1}(\mathbf{b}_\mu^+\mathbf{a})^2/(\mathbf{b}_\mu^+\mathsf{A}_1\mathbf{b}_\mu)$$

and the proof of property (5) is complete.

4. Numerical algorithm

As our experience has shown, the calculation of the moments (7.4) has to be performed very accurately. A scaling was introduced in order to avoid numerical singularities due to the large variations in the order of magnitude of the matrix elements of A_1 and A_2. The scaling was applied in the form

$$\mathsf{A}_2' = \mathsf{S}\mathsf{A}_2\mathsf{S}, \quad \mathsf{A}_1' = \mathsf{S}\mathsf{A}_1\mathsf{S}, \quad \mathbf{a}' = \mathsf{S}\mathbf{a},$$

where S is a diagonal matrix with the elements $s_{ii} = a_i$. The solution of the eigenvalue problem (7.11) may then be performed in the scaled vector space where the Frobenius form of the scaled matrix (7.10) is conserved. Using this special property one may evaluate the eigenvectors recursively from the eigenvalues.[19] In our setup a QR algorithm[20] was used to obtain the eigenvalues.

H. Approximate analytical description

In this section an approximate analytical expression for the CFM signal will be derived. The resulting expression exhibits a systematic error but, nevertheless, suffices for an estimate of the diffusion coefficient and photochemical rate constant. The application of the analytical approximation may be advantageous if a very fast analysis of the CFM signal is required.

The fluorophore distribution $P(\mathbf{r}, t)$ is governed by the diffusion-reaction equations (2.1) and (2.2). Let $P(\mathbf{r}, t\,|\mathbf{r}_0, t_0)$ denote the Green's function for this equation corresponding to the initial condition

$$P(\mathbf{r}, t = t_0|\mathbf{r}_0, t_0) = \delta(\mathbf{r} - \mathbf{r}_0). \tag{8.1}$$

The nonreactive Green's function for $k(\mathbf{r}) = 0$ is denoted by $P_0(\mathbf{r}, t\,|\mathbf{r}_0, t_0)$. This function obeys the adjoint equation

$$-\frac{\partial}{\partial t}P_0(\mathbf{r}_1, t_1|\mathbf{r}, t) = D\nabla_r^2 P_0(\mathbf{r}_1, t_1|\mathbf{r}, t) \tag{8.2}$$

with an initial condition like Eq. (8.1) and with boundary conditions like in Eq. (2.2). Multiplication of Eq. (2.1) by $P_0(\mathbf{r}_1, t_1|\mathbf{r}, t)$ and of Eq. (8.2) by $P(\mathbf{r}, t\,|\mathbf{r}_0 t_0)$, substraction and integration over t and $\mathbf{r}$ yields for the left-hand side

$$\begin{aligned}
&\int d^2r\int_{t_0}^{t_1} dt\left[P_0(\mathbf{r}_1, t_1|\mathbf{r}, t)\frac{\partial}{\partial t}P(\mathbf{r}, t\,|\mathbf{r}_0, t_0)\right.\\
&\quad\left. + P(\mathbf{r}, t\,|\mathbf{r}_0, t_0)\frac{\partial}{\partial t}P_0(\mathbf{r}_1, t_1|\mathbf{r}, t)\right]\\
&= \int d^2r[P_0(\mathbf{r}_1, t_1|\mathbf{r}, t_1)P(\mathbf{r}, t_1|\mathbf{r}_0, t_0)\\
&\quad - P_0(\mathbf{r}_1, t_1|\mathbf{r}, t_0)P(\mathbf{r}, t_0|\mathbf{r}_0, t_0)]\\
&= \int d^2r[\delta(\mathbf{r}_1 - \mathbf{r})P(\mathbf{r}, t_1|\mathbf{r}_0, t_0)\\
&\quad - P_0(\mathbf{r}_1, t_1|\mathbf{r}, t_0)\delta(\mathbf{r} - \mathbf{r}_0)]\\
&= P(\mathbf{r}_1, t_1|\mathbf{r}_0, t_0) - P_0(\mathbf{r}_1, t_1|\mathbf{r}_0, t_0).
\end{aligned}$$

For the right-hand side follows because of the self-adjointness of the Laplacian

$$\begin{aligned}
&\int d^2r\int_{t_0}^{t_1} dt\{P_0(\mathbf{r}_1, t_1|\mathbf{r}, t)[D\nabla^2 - k(\mathbf{r})]P(\mathbf{r}, t\,|\mathbf{r}_0, t_0)\\
&\quad - P(\mathbf{r}, t\,|\mathbf{r}_0, t_0)D\nabla^2 P_0(\mathbf{r}_1, t_1|\mathbf{r}, t)\}\\
&= -\int d^2r\int_{t_0}^{t_1} dt\, P_0(\mathbf{r}_1, t_1|\mathbf{r}, t)k(\mathbf{r})P(\mathbf{r}, t\,|\mathbf{r}_0, t_0).
\end{aligned}$$

Hence, one obtains the Lippman–Schwinger[25] equation

$$\begin{aligned}
P(\mathbf{r}, t\,|\mathbf{r}_0, t_0) &= P_0(\mathbf{r}, t\,|\mathbf{r}_0, t_0)\\
&\quad - \int_{t_0}^{t} dt'\int d^2r'\, P_0(\mathbf{r}, t\,|\mathbf{r}', t')k(\mathbf{r}')P(\mathbf{r}', t'|r_0, t_0).
\end{aligned}$$

This equation had been derived in Ref. 26 in a more general context. Average over the initial condition $f(\mathbf{r}_0) = 1$ yields with

$$\int d\mathbf{r}_0 f(\mathbf{r}_0)P(\mathbf{r}, t\,|\mathbf{r}_0, t_0) = P(\mathbf{r}, t),$$

$$\int d\mathbf{r}_0 f(\mathbf{r}_0)P_0(\mathbf{r}, t\,|\mathbf{r}_0, t_0) = 1,$$

the integral equation for the CFM distribution

$$P(\mathbf{r}, t) = 1 - \int_{t_0}^{t} dt'\int d^2r'\, P_0(\mathbf{r}, t\,|\mathbf{r}', t')k(\mathbf{r}')P(\mathbf{r}', t'). \tag{8.4}$$

The CFM signal is given by

$$N(t) = \int d^2r\, k(\mathbf{r})P(\mathbf{r}, t). \tag{8.5}$$

If one assumes in analogy to an approximation introduced by Wilemski and Fixman[27] that

$$\int d^2r\, k(\mathbf{r})P_0(\mathbf{r}, t\,|\mathbf{r}', t') = g(\mathbf{r}', t - t')$$

is independent of $\mathbf{r}'$ over the domain where $k(\mathbf{r}') \neq 0$ one arrives at the approximation

$$N(t)\approx K-\int_{t_0}^{t}dt'\,S(t-t')N(t') \tag{8.6}$$

with

$$S(t-t')=(1/K)\int d^2r\int d^2r'\,k(\mathbf{r})P_0(\mathbf{r},t\,|\mathbf{r}',t')k(\mathbf{r}') \tag{8.7}$$

and

$$K=\int d^2r\,k(\mathbf{r}). \tag{8.8}$$

The approximation involves the neglect of the term

$$\int_{t_0}^{t}dt'\int d^2r\,k(\mathbf{r})P_0(\mathbf{r},t\,|\mathbf{r}',t')k(\mathbf{r}')[P(\mathbf{r}',t')-\hat{P}(t')], \tag{8.9}$$

where

$$\hat{P}(t')=\frac{\int d^2r'\,P(\mathbf{r}',t')k(\mathbf{r}')}{\int d^2r'\,k(\mathbf{r}')}. \tag{8.10}$$

This is the only approximation introduced here. This assumption cannot be improved systematically which is the reason why the expression arrived at in the following cannot be improved in a straightforward way.

From Eq. (8.6) one obtains with $t_0=0$,

$$N(0)=K,$$

$$\frac{\partial}{\partial t}N(0)=-S(0)N(0)=-\int d^2r\,k^2(r),$$

which is an exact relationship as can be shown considering the limit $t\to 0$ of the formal solution

$$N(t)=\int d^2r\,k(\mathbf{r})\exp\{t\,[D\nabla^2-k(\mathbf{r})]\}f(\mathbf{r}) \tag{8.11}$$

with $f(\mathbf{r})=1$.

The free particle correlation function $S(t-t')$ can be evaluated as follows. The free particle Green's function can be written

$$\begin{aligned}P_0(\mathbf{r},t\,|\mathbf{r}'0)&=(4Dt\pi)^{-1}\exp[-(\mathbf{r}-\mathbf{r}')^2/(4Dt)]\\&=(4Dt\pi)^{-1}\exp[-r^2/(4Dt)]\\&\quad\times\exp[-r'^2/(4Dt)]J,\end{aligned} \tag{8.12}$$

where[28]

$$\begin{aligned}J&=\exp[rr'\cos(\phi-\phi')/(2Dt)]\\&=I_0(z)+2\sum_{k=1}^{\infty}I_k(z)\cos[k(\phi-\phi')]\end{aligned} \tag{8.13}$$

with $z=rr'/(2Dt)$, azimuthal angles ϕ,ϕ', and I_k representing the modified Bessel functions. Since $k(\mathbf{r})$ is radially symmetric, evaluation of $S(t-t')$ involves an azimuthal average of J over ϕ–ϕ' and, hence, only the leading term in the above series expansion contributes. Therefore,

$$\begin{aligned}S(t)&=\frac{4\pi}{4DtK}\int rdr\int r'dr'\,k(r')k(r)\\&\quad\times\exp\left(\frac{-r^2}{4Dt}\right)I_0\left(\frac{rr'}{2Dt}\right)\exp\left(\frac{-r'^2}{4Dt}\right).\end{aligned} \tag{8.14}$$

Employing the expansion[28]

$$I_0(z)=1+\frac{(z/2)^2}{(1!)^2}+\frac{(z/2)^4}{(2!)^2}+\cdots, \tag{8.15}$$

one obtains

$$S(t)=(4\pi Dt/K)\sum_{n=0}^{\infty}S_n^2(t), \tag{8.16}$$

$$S_n(t)=(1/n!)\int dy\,y^n\,\exp(-y)k(\sqrt{4Dty}). \tag{8.17}$$

In case of a Gaussian $k(\mathbf{r})$ [see Eq. (2.5)] one can evaluate $S(t)$ in a closed form. One first obtains

$$\begin{aligned}K&=\pi a^2k_0,\\S_n&=2k_0/(1+8Dt/a^2)^{n+1},\end{aligned} \tag{8.18}$$

from which one arrives at

$$S(t)=k_0/(1+4Dt/a^2).$$

In case of a rectangular $k(\mathbf{r})$ [see Eq. (2.4)] one evaluates

$$K=\pi a^2k_0 \tag{8.20}$$

and

$$\begin{aligned}S(t)&=(4Dtk_0/a^2)\sum_{n=0}^{\infty}\sigma_n^2(a^2/[4Dt\,]),\\\sigma_n(x)&=(1/n!)\int_0^x dy\,y^n\,\exp(-y).\end{aligned} \tag{8.21}$$

For $n\geqslant 1$ holds

$$\int_0^x dy\,y^n\,\exp(-y)=-x^n\,\exp(-x)+n!\sigma_{n-1}(x)$$

or

$$\begin{aligned}\sigma_n(x)&=-x^n\,\exp(-x)/n!+\sigma_{n-1}(x),\\\sigma_0(x)&=1-\exp(-x),\end{aligned} \tag{8.22}$$

which provides a recursive algorithm for the evaluation of $\sigma_n(x)$. The asymptotic behavior

$$\begin{aligned}S(t)&\underset{t\to\infty}{\sim}(4Dtk_0/a^2)\{1-\exp[-a^2/(4Dt)]\}^2\\&\approx k_0a^2/(4Dt)\end{aligned}$$

agrees with that of the Gaussian profile for identical radiation dose K.

The analytical expressions for $S(t)$ provide a simple algorithm to determine the CFM signal (8.5) by means of the approximation (8.6). For this purpose one discretizes the integral in Eq. (8.6) and employs the appropriate expression for $S(t)$.

The accuracy of the CFM signal (8.6) with $S(t)$ evaluated according to the expansion (8.21) for a rectangular profile is shown in Fig. 1. One observes from the comparison with the exact fluorescence decay evaluated by the Crank–Nicholson scheme that the approximate $N(t)$ underestimates the CFM signal. The small deviation shown in Fig. 1 is typical for most applications and, therefore, one may employ the approximate $N(t)$ to fit CFM experiments and, thereby, determine diffusion coefficients. In particular, one may employ

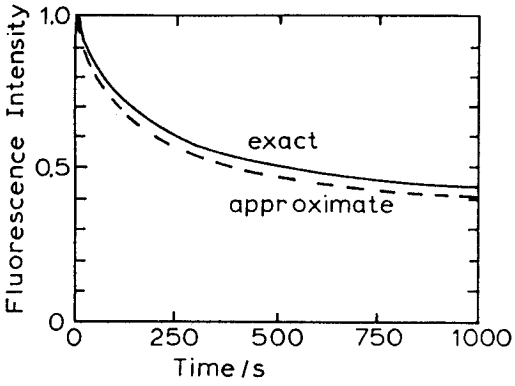

FIG. 1. Comparison of exact and approximate [Eqs. (8.6) and (8.21)] fluorescence decay signals evaluated for $a = 2.0\ \mu m$, $D = 0.009\ \mu m^2\ s^{-1}$, $k_0 = 0.005\ s^{-1}$ and $R = 20\ \mu m$. The exact fluorescence decay was determined by means of the Crank–Nicholson scheme described in Sec. II E.

the approximate expression in a first phase of the fitting procedure and invoke the more time-consuming exact evaluation of the CFM signal only for an exact matching of theoretical and experimental decay curves. We note finally that the approximation is rather poor for the case of a Gaussian profile $k(\mathbf{r})$ since in this case the assumption made in the derivation above of an $\mathbf{r}'$-independent $g(\mathbf{r}', t - t')$ is too crude.

III. RESULTS

A. Comparison of FM and CFM measurements

In a typical application of the CFM method one measures the fluorescence decay during illumination at a constant light level and fits the decay curve to the theoretical description, thereby, obtaining the diffusion coefficient of the fluorophore.[13] As a demonstration of the accuracy and applicability of the CFM method we will provide a comparison of measurements of diffusion coefficients D in membranes and glycerol/water systems with D values ranging between 0.001 and 10.0 $\mu m^2\ s^{-1}$. FM measurements were evaluated by reading the half-time of fluorescence recovery from the measuring curve and inserting it into Eq. (19) of Ref. 2.

One possible realization of a system with greatly different diffusion coefficients is provided by a phospholipid multibilayer system around a temperature-induced phase transition. The structural changes of phase transitions are accompanied by changes in the membrane viscosity, i.e., rotational and translational diffusion coefficients, by several orders of magnitude.[29,30] To explain these phase transitions one assumes a transformation of the lipid bilayer from an ordered crystalline phase in two dimensions into a partially fluid phase where the polar groups are still ordered but the aliphatic chains become disordered.[31]

Figure 2a compares CFM and FM measurements on the artificial membrane of dimyrostoylphosphatidylcholine (DMPC) at the well known phase transition near 24 °C of this system which produces a viscosity change by four orders of magnitude. The CFM and FM measurements coincide for temperatures in which the bilayer is in a fluid state, i.e., above 24 °C. Below 24 °C the bilayer decomposes into crystalline domains (D about $10^{-6}\ \mu m^2\ s^{-1}$) and structural defects (D about $0.1\ \mu m^2\ s^{-1}$). The fraction of crystalline domains is a function of temperature amounting to 80%–90% in the 10–24 °C range.[32] The diffusion coefficients given in Fig. 2a for temperatures smaller than 24 °C are average values of the slow and fast component. The FM values are markedly larger than the CFM values. This is presumably due to the different types of data evaluation used in FM and CFM experiments. In the FM experiment the half-time of fluorescence recovery, i.e., a parameter of the early time regime, was used to compute the diffusion thereby emphasizing the fast component. In CFM experiments the fluorescence decay was fitted over a considerable time interval (10–20 half-times) thus putting more weight on the slow component.

Figures 2(b) and 2(c) illustrate the fluorophore decay for the case of high and low viscosity below and above the phase transition at temperatues of 18 and 34 °C, respectively. These figures show that both in the high and low viscosity limit a satisfactory fit is obtained between the observations and the theoretical decay curves thereby yielding the diffusion coefficients presented in Fig. 2(a).

In order to test the CFM methods for intermediate diffusion coefficients we investigated the above membrane system when half of the DMPC material was replaced by cholesterol. The CFM and FM measurements agree for this system as shown in Fig. 2(a). The measurements for both systems involved the dye *N*-4-nitrobenzo-2-oxa-1,3 diazole egg phosphatidylethanolamine which because of its size extends from the water interface to the center of the bilayer. We have investigated the DMPC/cholesterol system also with the smaller diphenylhexatriene chromophore which is expected to reside in the more fluid center of the bilayer. Figure 2(a) shows that this chromophore does, in fact, exhibit a larger diffusion coefficient.

Also to cover systems with diffusion coefficients in the range around $0.1\ \mu m^2\ s^{-1}$ we have investigated the dye-labeled protein fluoresceineisothiocyanate–bovine serum albumine in a glycerol/water mixture. The diffusion coefficients determined by the CFM and the FM method are found to agree closely as shown in Fig. 2(a).

B. Comparison of rectangular and Gaussian intensity profile

In Fig. 3 the predicted time development of the dye distribution $P(r, t)$ for a Gaussian intensity profile and a flat membrane is shown. Initially, the fluorophore concentration is constant throughout. The photoreaction decreases the concentration in the IA. Diffusion tends to replenish the fluorophores in the IA whereby the concentration in the surroundings slowly decreases. Compared to the distributions of a rectangular intensity profile (cf. Fig. 3 in Ref. 13) the distributions show some characteristics of a Gaussian function. However, as depicted in Fig. 4., the fluorescence decay curves show little difference between the Gaussian and a rectangular intensity profile of identical radiation dose as long as the k_0/D ratio is not too large. The positive deviations shown in Fig. 4 are caused by the areas of low intensity of a Gaussian profile where the fluorophore decay is slow. For smaller k_0/D ratios this effect is suppressed by the domi-

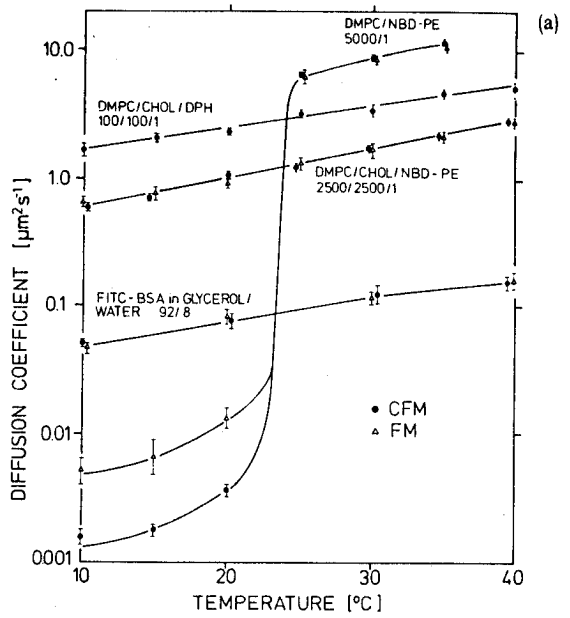

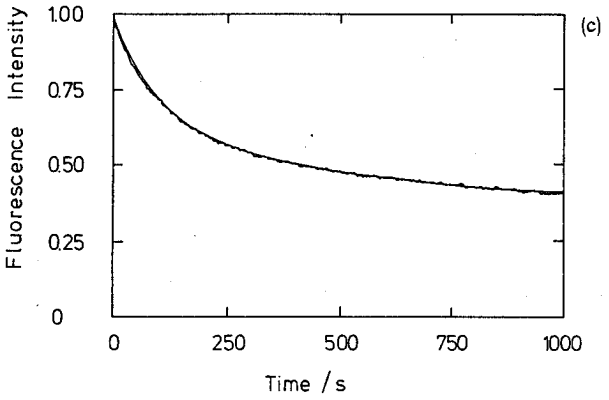

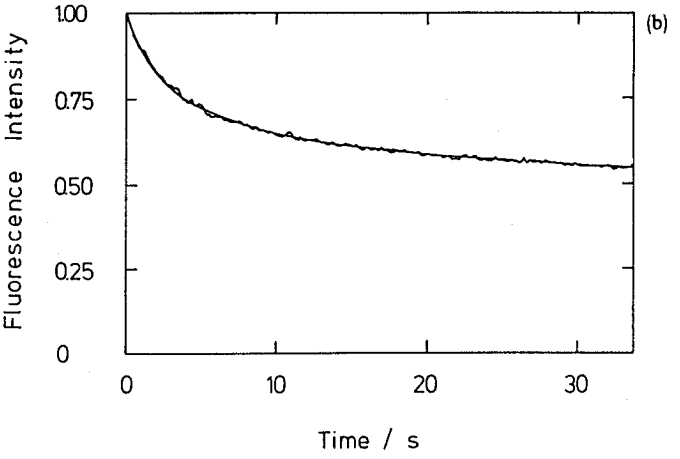

FIG. 2. (a) Comparison of FM and CFM measurements on three systems; (1) dimyrostoylphosphatidylcholine DMPC with the fluorophore *N*-4-nitrobenzo-2-oxa-1,3 diazole egg phosphatidylethanolamine in a 5000:1 molar ratio; this system exhibits a phase transition at 24 °C; (2) a DMPC cholesterol (CHOL) system with an NBD-PE fluorophore in a 2500:2500:1 molar ratio; (3) a dye-labeled protein fluoresceinisothiocyanate–bovine serum albumine (FITC-BSA) in a glycerol/water mixture of 92:8 weight ratio; also shown is a DMPC/CHOL system with the fluorophore diphenylhexatriene (DPH) in a 100:100:1 molar ratio; the error bars shown result from the mean $\pm$ *S.D.* of 5–10 measurements. (b) comparison of observed and calculated fluorescence decay corresponding to a CFM measurement of the DMPC system in Fig. 2(a) below the phase transition at 18 °C with the fluorescence lipid analog 3,3'-dioctadecyloxatricarbocyanine; the radius of the irradiated area (IA) was $a = 2.0$ μm; the theoretical curve corresponds to $k_0 = 0.005\,s^{-1}$ and $D = 0.009\,\mu m^2\,s^{-1}$ ($R = 20.0\,\mu$m). (c) Same as (b), however, measurement above the phase transition of the DMPC system at 34 °C; the radius of the irradiated area was $a = 8\,\mu$m; the theoretical curve corresponds to $k_0 = 0.19\,s^{-1}$ and $D = 12.0\,\mu m^2\,s^{-1}$ ($R = 80.0\,\mu$m, Crank–Nicholson scheme).

nant diffusion. For all practical purposes CFM measurements may be arranged to produce a curve similar to (b) with characteristic reaction time $1/k_0$ similar to the characteristic diffusion time a^2/D through the IA[13] and the difference between a Gaussian and a rectangular intensity profile may be neglected for the analysis.

C. Comparison of flat and spherical membranes

The influence of the three-dimensional membrane geometry on the CFM measurements was probed by comparing model calculations on a flat and a spherical surface. As Fig. 5 shows there are little deviations between the two geometries as long as the size of the IA as well as of the diffusion area are identical for the two geometries. This is even true for the case that a half-sphere and a planar, circular region is irradiated [case (b) in Fig. 5], i.e., in the limit that the size of

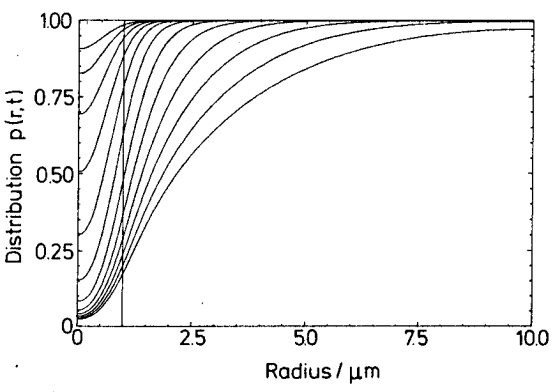

FIG. 3. Time dependence of the dye distribution function $P(r, t)$ in case of irradiation with a Gaussian intensity profile ($a = 1$ μm, $R = 10$ μm, $k_0 = 1.0\,s^{-1}$ and $D = 0.1\,\mu m^2\,s^{-1}$, Crank–Nicholson scheme); the distributions are taken at successive times 0.05 * 2^n s. $n = 0, 1, \ldots, 11$; the spatial extend of the IA is indicated.

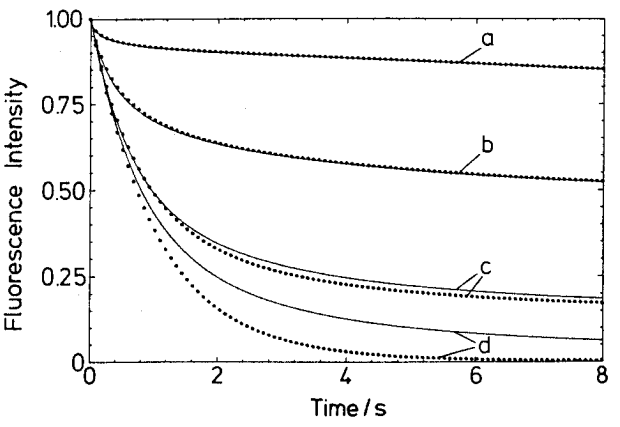

FIG. 4. Comparison of the fluorescence decay for Gaussian (—) and rectangular (. . .) intensity profiles of identical radiation doses for various diffusion coefficients, (a) $D = 10.0$ $\mu m^2\,s^{-1}$, (b) $D = 1.0$ $\mu m^2\,s^{-1}$, (c) $D = 0.1$ $\mu m^2\,s^{-1}$, (d) $D = 0.0001$ $\mu m^2\,s^{-1}$, ($k_0 = 1$ s^{-1}, $a = 1$ μm, $R = 10$ μm, Crank–Nicholson scheme).

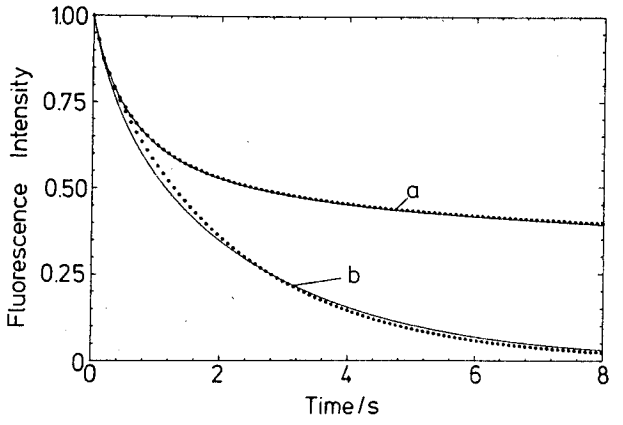

FIG. 5. Comparison of the fluorescence decay for diffusion on a sphere (—) and in a plane (. . .) for identical areas of the IA and of the diffusion space. (a) $\theta_a = 0.142$ rad, $\theta_R = 1.57$ rad, $S = 7.05\,\mu$m (sphere) and $a = 1\,\mu$m, $R = 10\,\mu$m (plane); (b) $\theta_a = 1.57$ rad, $\theta_R = 3.14$ rad, $S = 0.71\,\mu$m (sphere) and $a = 1\,\mu$m, $R = 1.41\,\mu$m (plane); ($k_0 = 1\ s^{-1}$, $D = 0.5\,\mu m^2\,s^{-1}$, Crank–Nicholson scheme).

the IA is half of the respective diffusion space for the two geometries. The slight deviations (first negative and then positive) can be explained as follows. The circumference of the IA is shorter for the spherical geometry than for the planar geometry and, therefore, fewer fluorophores can enter the IA in a certain time interval. This results in an initial, faster fluorescence decay of the IA, but since the total number of fluorophores decreases slower a break-even point will be reached when more fluorophores are inside the IA and contribute to the fluorescence signal.

As the results in Fig. 5 show, there is little influence of the membrane geometry on the CFM decay curves. This is illustrated in Fig. 6 where the time-dependent fluorescence decay during the CFM of DiO labeled erythrocyte cells is depicted. The theoretical analysis with flat as well as with spherical geometries approximately gives identical results with a diffusion coefficient of $D = 0.32\,\mu m^2\,s^{-1}$ and a reaction rate constant $k_0 = 2.0\ s^{-1}$. This measurement is difficult to perform with the conventional FM technique due to cell damage caused by the strong FM photolysis. Comparable data on isolated erythrocyte membranes (ghosts) predict $D \approx 0.2$–$0.3\,\mu m^2\,s^{-1}$.[6]

D. Simulation of conventional FM experiments

Conventional photobleaching experiments involve a time-varying laser profile in the IA. An initial intense laser beam bleaches essentially all fluorophores in the IA. In a second recovery phase of the experiment an attenuated laser beam monitores the transport of nonphotolyzed fluorophores into the IA. During this phase the fluorescence signal recovers from a zero value back to a fluorescence level which, in general, is identical to the initial fluorescence level before the bleaching phase. As already mentioned in Sec. II E, the Crank–Nicholson scheme allows us to introduce a time dependence of the photochemical rate constant in the diffusion-reaction system and, therefore, can also describe the FM experiment. As an application of the theory we simulate a conventional FM experiment for the case in which the fluorescence intensity does not return to the initial intensity. Such behavior has been observed in many cases. The question arises if this behavior is due to a certain immobile fraction of dye-labeled lipids or if it may be due to a finite-size diffusion space such that the bleaching period of the FM method bleaches a nonnegligible fraction of available fluorophores. In particular, one wishes to examine whether the observed fluorescence recovery curves allow to distinguish between these two possibilities. In Fig. 7(b) we have simulated an FM experiment assuming the existence of an immobile fraction of fluorophores. In Fig. 7(a) no immobile fraction has been assumed but the diffusion space has been limited to a relatively small area. Therefore, the total number of fluorophores is reduced to 72% after the FM photobleaching. The diffusion coefficient for case (a) was chosen such that the recovery curve compares to that of case (b) as closely as possible. The good comparison shows FM experiments with partial fluorescence recovery cannot distinguish between a limited diffusion space and an immobile fraction of fluorophores. It should be noted that case (a) represents a FM con-

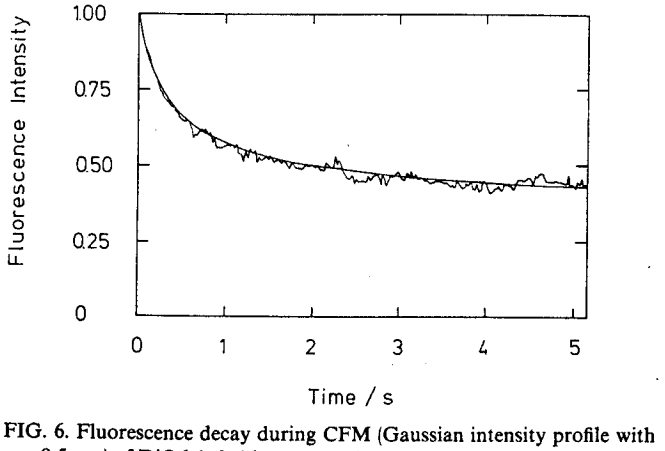

FIG. 6. Fluorescence decay during CFM (Gaussian intensity profile with $a = 0.5\,\mu$m) of DiO labeled human erythrocyte cells (50 μl human blood; washed several times; incubation in isotonic medium, phosphate buffer pH 7.6, 50 μg/ml DiO, dimethylsulfoxid 2.5 Vol %; 15 min, 37 °C); the fitted curve corresponds to $k_0 = 2.0\ s^{-1}$ and $D = 0.32\,\mu m^2 s^{-1}$ and applies in good approximation to a flat ($R = 5.0\,\mu$m) as well as to a spherical membrane ($\theta_a = 0.15$ rad, $\theta_R = 1.57$ rad, $S = 3.22\,\mu$m, Crank–Nicholson scheme).

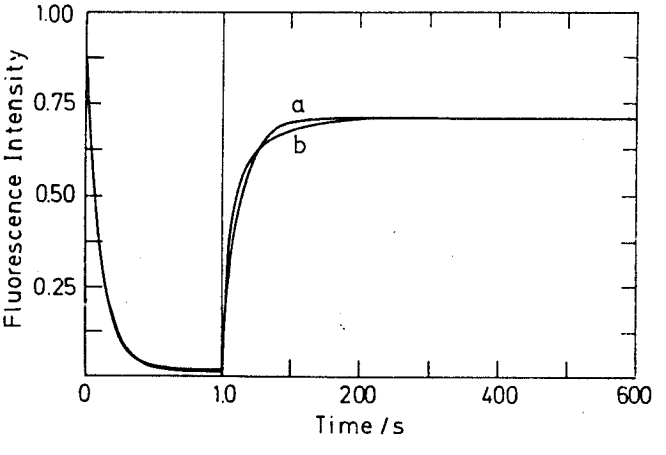

FIG. 7. Numerical simulation (Crank–Nicholson scheme) of a conventional FM measurement; the fluorescence bleaching extends over 1 s, the consecutive fluorescence recovery extends over 600 s (note different times scales!). Cuve (a): $R = 20\,\mu$m and $D = 1.0\,\mu m^2\,s^{-1}$, curve (b): $R = 50\,\mu$m, $D = 3.0\,\mu m^2\,s^{-1}$ and 25% immobile fraction; [$k_0(0 < t < 1.0\,s) = 10.0\,s^{-1}$, rectangular intensity profile, $a = 10\,\mu$m].

dition not suitable for the mathematical analysis developed, for instance, in Ref. 2.

E. Convergence of the generalized moment expansion

In Figs. 8(a), 8(b), and 8(c) several generalized moment expansions for the fluorescence decay of a representative CFM simulation are depicted and compared with the exact solution of Eq. (2.1) obtained by application of the methods described in Sec. II E. As Fig. 8(a) shows the expansion involving eight long time and eight short time moments agrees well with the exact solution. The contribution of the long time moments appears to be more important for the present problem than the contribution of the short time moments as can be seen in Fig. 8(b) which compares the descriptions for the limiting cases that either eight short or eight long time moments are considered. Finally, Fig. 8(c) represents a description which includes two short time and six long time moments, and which gives sufficient accuracy for an analysis of the experimental data. Compared to the Crank–Nicholson scheme the generalized moment expansion performs faster by about a factor 10.

F. Implementation and numerical convergence

The calculations were performed on a SPERRY UNIVAC 1100/82, a CDC CYBER 175, a PDP 11/23, a VAX 11/750, and a HP 85 top desk computer. The algorithms were written in standard ANSI FORTRAN-77 and may be implemented with minor modifications on main frame computers as well as on lab microprocessors. For the Crank–Nicholson scheme there is also a BASIC version available.

For a numerical convergence of the spatial discretization (see the Appendix) of better than 1% the grid parameter u was set to 12 and h was set to 0.0003. For the time steps τ of the Crank–Nicholson scheme an empirical formula was developed,

$$\tau \leqslant \min[0.08 A_{IA}/(\pi D), 0.05/k_0],$$

where A_{IA} is the area of the IA given by $A_{IA} = \pi a^2$ for the planar case and $A_{IA} = 2\pi S^2(1 - \cos\theta_a)$ for the spherical case. In most cases the experimental photon count interval already fulfills this formula. A fit which was in reasonable agreement with the experimental curve could be obtained after typically five to ten calculations. The fit was performed interactively on a graphics terminal.

ACKNOWLEDGMENTS

We would like to thank Zan Schulten for valuable suggestions. This work has been supported by the Deutsche Forschungsgemeinschaft (SFB-143 C1).

APPENDIX

I. Discretization for the planar case

In the following, the dimensionless units

$$r \to r/r_0, \quad t \to t/t_0, \quad t_0 = r_0^2/D$$

are chosen where $a = r_0(u - 1)$ is a measure for the coarseness of the equidistant discretization of the spatial coordinate r,

$$r_j = (j - 1) + h, \quad j = 1, \ldots, n, \quad r_n = R/r_0, \quad h \ll 1,$$

and u is the lattice point corresponding to the radius a.

In order to avoid a singular behavior of the matrix L defined below one has to chose $r_1 = h \neq 0$. The difference approximation of the diffusion operator $l(r)$ was performed similar to Refs. 16, 17, and 18 and yields a nonsymmetric tridiagonal matrix L which approximates the continuous op-

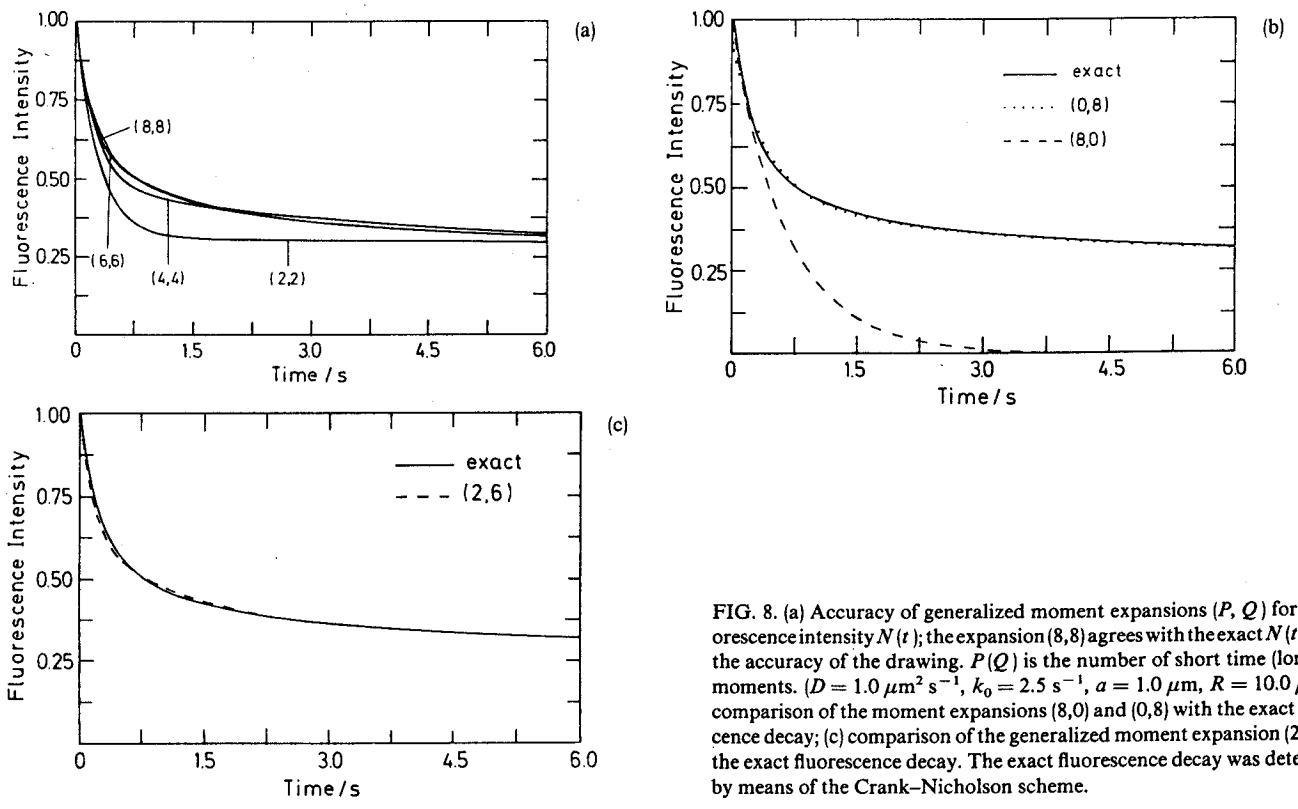

FIG. 8. (a) Accuracy of generalized moment expansions (P, Q) for the fluorescence intensity $N(t)$; the expansion (8,8) agrees with the exact $N(t)$ within the accuracy of the drawing. $P(Q)$ is the number of short time (long time) moments. ($D = 1.0\ \mu m^2\ s^{-1}$, $k_0 = 2.5\ s^{-1}$, $a = 1.0\ \mu m$, $R = 10.0\ \mu m$); (b) comparison of the moment expansions (8,0) and (0,8) with the exact fluorescence decay; (c) comparison of the generalized moment expansion (2.6) with the exact fluorescence decay. The exact fluorescence decay was determined by means of the Crank–Nicholson scheme.

erator up to second order in r_0:

$$\begin{aligned} L_{jj\pm1} &= 1 \pm 1/(2r_j), \\ L_{jj} &= -2, \\ -L_{11} &= L_{12} = 2 + 1/r_1, \\ -L_{nn} &= L_{nn-1} = 2 - 1/r_n, \end{aligned} \tag{A1}$$

where $j = 2, \ldots, n-1$. Application of the trapezoidal rule to the Riemann integral of the observable $N(t)$ in Eq. (2.8) gives the summation weights in Eq. (3.1b),

$$\eta_j = r_i \omega_i \Big/ \Big(\sum_{j=1}^{n} \omega_j k_{ij} r_j \Big), \tag{A2}$$

where $\omega_i = 1$ for $i = 2, \ldots, n-1$ and $\omega_i = 0.5$ for $i = 1, n$. Similarly, one obtains for the total number of fluorophores,

$$N_{\text{tot}}(t) = 2\pi \sum_{i=1}^{n} r_i \omega_i P_i(t).$$

The operator L is constructed in such a way that $N_{\text{tot}}(t)$ is an invariant of the reaction-free (K = 0) problem (3.1a),

$$\frac{\partial}{\partial t} N_{\text{tot}}(t) = 2\pi \sum_{j=1}^{n} \sum_{i=1}^{n} r_i \omega_i L_{ij} P_j(t) = 0. \tag{A3}$$

Hence, Eq. (A3) provides a suitable choice for the reflective boundary conditions at $r = r_1$ and $r = R$.

As is shown in Sec. II D, the operator L can be symmetrized by a similarity transformation and, therefore, has only real eigenvalues. A simple application of the Gerschgorin theorem[19] shows that L is negative semidefinite. The relation (A3) requires the existence of a zero eigenvalue and P(0) is the correspondign eigenvector, i.e.,

$$\mathbf{L}\mathbf{P}(0) = 0. \tag{A4}$$

Furthermore, the operator L fulfills the detailed balance condition

$$L_{ji}\eta_j = L_{ij}\eta_i, \; i,j = 1, \ldots, n. \tag{A5}$$

The (scalar) reaction operator $k(r)$ in Eq. (3.1a) corresponds to a diagonal matrix K with the diagonal elements

$$K_{jj} = \begin{cases} k_0 t_0 & j = 1, 2, \ldots, u-1 \\ k_0 t_0/2 & j = u \\ 0 & j = u+1, \ldots, n \end{cases} \quad \text{(rectangular profile)},$$

$$K_{jj} = 2t_0 k_0 \exp[-2r_j^2/(r_u - 1)^2] \quad \text{(Gaussian profile)}, \tag{A6}$$

where the factor 1/2 in the uth diagonal element was introduced empirically to improve the convergence to order r_0^2.

2. Discretization for the spherical case

Similar to the planar case dimensionless units

$$t \to t/t_0, \; t_0 = S^2/D$$

and the equidistant discretization

$$r_i = -1 + (i-1)\delta, \; i = 1, \ldots, n, \quad r_n = R < 1$$

are chosen. The nonsymmetric tridiagonal matrix L contains now the elements

$$\begin{aligned} L_{jj\pm1} &= (1/\delta^2)(1 - r_j^2) \mp r_j/\delta, \\ L_{jj} &= -(2/\delta^2)(1 - r_j^2), \\ -L_{11} &= L_{12} = 2/\delta, \\ -L_{nn} &= L_{nn-1} = -2L_{n-1n-1} - 2L_{n-2n-1} \\ &= (2/\delta^2)(1 - r_n^2) + 2r_n/\delta, \end{aligned}$$

where $j = 2, \ldots, n-1$. The summation weights are chosen as

$$\eta = \omega_i \Big/ \Big(\sum_{j=1}^{n} \omega_j k_{ij} \Big),$$

where $\omega_i = 1$ for $i = 2, \ldots, n-1$ and $\omega_i = 0.5$ for $i = 1, n$. The matrix L conserves the total number of fluorophores,

$$\frac{\partial}{\partial t} N_{\text{tot}}(t) = 2\pi S^2 \delta \sum_{j=1}^{n} \sum_{i=1}^{n} \omega_i L_{ij} P_j(t) = 0.$$

Again, P(0) is the stationary solution of the reaction-free problem and the detailed balance condition (A5) is fulfilled. The definition of the rectangular intensity profile is identical to Eq. (A6) whereas the Gaussian profile is defined as

$$K_{ij} = 2t_0 k_0 \exp[-2(1 + r_j)/(1 + a)].$$

[1] R. Peters, J. Peters, K. H. Tews, and W. Bähr, Biochim. Biophys. Acta **367**, 282 (1974).
[2] D. Axelrod, D. E. Koppel, J. Schlessinger, E. Elson, and W. W. Webb, Biophys. J. **16**, 1055 (1976).
[3] R. Peters, J. Biol. Chem. **258**, 1147 (1983).
[4] K. Jacobson, E. Elson, D. Koppel, and W. W. Webb, Nature **295**, 283 (1982).
[5] S. J. Singer and G. L. Nicholson, Science **175**, 720 (1972).
[6] H.-G. Kapitza and E. Sackmann, Biochim. Biophys. Acta **595**, 56 (1980).
[7] C. S. Yang, Life Sci. **21**, 1047 (1977).
[8] G. Riman, E. Hanski, and S. Braun, Nature **276**, 394 (1978).
[9] J. Schlessinger, TIBS **1980**, 210.
[10] D. M. Soumpasis, Biophys. J. **41**, 95 (1983).
[11] E. J. J. van Zoelen, L. G. J. Tertoolen, and S. W. Laat, Biophys. J. **42**, 103 (1983).
[12] B. A. Smith and H. M. McConnell, Proc. Natl. Acad. Sci. U.S.A. **75**, 2759 (1978).
[13] R. Peters, A. Brünger, and K. Schulten, Proc. Natl. Acad. Sci. U.S.A. **78**, 962 (1981).
[14] W. L. C. Vaz, M. Criado, V. M. C. Madeira, G. Schoellmann, and Th. Jovin, Biochem. **21**, 5608 (1982).
[15] P. G. Saffmann and M. Delbrück, Proc. Natl. Acad. Sci. U.S.A. **72**, 3111 (1975).
[16] R. D. Richtmeyer and K. W. Morton, *Difference Methods for Initial Value Problems* (Wiley, New York, 1967), pp. 189 and 198.
[17] Z. Schulten and K. Schulten, J. Chem. Phys. **66**, 4616 (1977).
[18] G. P. Zientara and F. H. Freed, J. Chem. Phys. **71**, 3861 (1979).
[19] J. Stoer and R. Bulirsch, *Introduction to Numerical Analysis* (Springer, New York, 1980), Chap. 6.
[20] (a) B. T. Smith, J. M. Boyle, B. S. Garbow, Y. Ikebe, V. C. Klema, and G. B. Moler, *Lecture Notes in Computer Science, Matrix Eigensystem Routines. EISPACK Guide Book*, 2nd ed. (Springer, New York, 1976); (b) IMSL Inc. Library Reference Manual, Houston, 1981.
[21] A. Szabo, K. Schulten, and Z. Schulten, J. Chem. Phys. **72**, 4350 (1980).
[22] O. Goscinski and E. Brändas, Int. J. Quantum Chem. **5**, 131 (1971).
[23] H. Mori, Prog. Theor. Phys. **34**, 399 (1965).
[24] K. Schulten, A. Brünger, W. Nadler, and Z. Schulten, in *Synergetics/From Microscopic to Macroscopic Order*, edited by E. Frehland (Springer, Berlin, 1984), p. 80.
[25] L. I. Schiff, *Quantum Mechanics*, 3rd ed. (McGraw-Hill, New York, 1968).
[26] G. Lamm and K. Schulten, J. Chem. Phys. **78**, 2713 (1983).
[27] G. Wilemski and M. Fixman, J. Chem. Phys. **58**, 4009 (1973); P. G. De Gennes, *ibid.* **76**, 3316 (1982); G. H. Weiss, *ibid.* **80**, 2880 (1984).
[28] M. Abramowitz and I. A. Stegun, *Handbook of Mathematical Functions* (Dover, New York, 1972).
[29] E.-S. Wu, K. Jacobson, and D. Papahadjopoulos, Biochemistry **16**, 3936 (1977).
[30] P. F. Fahey and W. W. Webb, Biochemistry **17**, 3046 (1978).
[31] M. K. Jain, in *Membrane Fluidity in Biology*, edited by R. C. Aloia (Adacemic, New York, 1983), Vol. 1, p. 1.
[32] H. G. Kapitza, D. A. Rüppel, H.-J. Galla, and E. Sackmann, Biophys. J. **45**, 577 (1984).